Submit   Log in   Register   Subscribe   Claim

| This journal | Journals | Publish | News & events | About | Search for... | Advanced search |

PDF   Figures   Save   Share

Reprints   Request

⬇ Download Full Issue

Fracturing with Carbon Dioxide: From Microscopic Mechanism to Reservoir Application

Xuehang Song [5] • Yintong Guo [5] • Jin Zhang [5] • ... Xiaofeng Li • Jinhui Zhou • Zhenqian Xue • Show all authors • Show footnotes

Check for updates

PlumX Metrics

Highlights

H
i
g
h

- CO_2 fracturing is more effective in reservoir stimulation than water

- Multiscale mechanism of CO_2 fracturing was experimentally established

- 4- to 20-fold increase in tight oil production was achieved by CO_2 fracturing

Context & Scale

As compared with conventional gas and oil reservoirs, low porosity and low permeability are the major obstacles for the recovery of unconventional resources. Therefore, reservoir fracturing by water was generally employed to stimulate production. However, alternative fracturing fluids are highly desired because of water shortage and pollution issues; therefore, dry CO_2 fracturing was proposed. Our multiscale investigation, from microscopic study to field tests, demonstrated that under reservoir conditions, injection pressures can be delivered into a larger reservoir matrix by CO_2, thus effectively lowering the fracturing pressure. More importantly, complex fracture networks can be generated together with greater stimulated reservoir volume. Eventually, enhanced production of unconventional resources can be achieved.

Summary

Water fracturing is widely employed as a reservoir-stimulating technology for the recovery of unconventional oil and gas. However, the process suffers from massive water consumption and environmental concerns. Therefore, alternative fracturing fluids are desired. In recent years, fracturing with CO_2 was proposed to embrace multiple benefits, including carbon storage, enhanced recovery, etc. Herein, based on specially designed facilities and new analytical methodologies, we present multiscale and quantitative investigations on the fracturing mechanism and behavior of CO_2 and water. It was demonstrated that because of the high leak-off of CO_2, shear fractures can be readily induced, which facilitated the formation of tensile and mixed fractures, leading to effective fracturing, complex networks, and greater stimulated reservoir volume. Finally, a 4- to 20- fold increase in tight oil production could be achieved by CO_2 fracturing in field tests with five wells.

Graphical Abstract
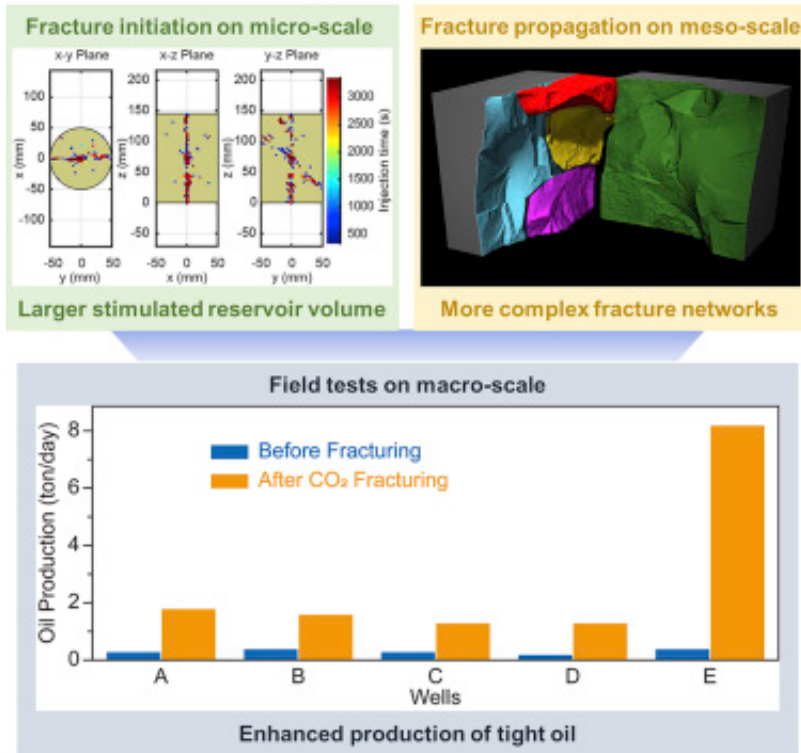
View Large Image | Figure Viewer | Download Hi-res image | Download (PPT)

Keywords

fracturing · carbon dioxide · shale gas · tight oil · field test

Introduction

Unconventional oil/gas is playing a more and more decisive role in the global energy market. In 2015, more than half of gas and oil production in North

American was contributed from shale and tight reservoirs.[1] The global abundance of unconventional oil/gas may shift the energy consumption structure from coal to less-carbon-intensive resources, and as concluded by several life-cycle assessments, such transformation opens up an alternative approach for decarbonization and reduction of greenhouse gas emission.[2, 3, 4] However, most of the unconventional oil/gas reservoirs are characterized by low porosity and low permeability, requiring reservoir stimulation technologies such as formation reconstruction to enable commercial production. Currently, water fracturing has been well established and deployed, particularly in the North American shale gas recovery. However, a huge amount of water is needed in such a process, which has already become an issue in Texas, North Dakota, Kansas, etc.[5] There are other concerns related to water fracturing. For example, swelling of clay minerals by water can significantly damage diffusion channels, greatly decrease the impact of water fracturing, and thus lead to poor production.[5, 6] Meanwhile, during the early stage of production, most of the used water and some of the underground water usually flow back to the surface, which is contaminated by hazardous substances from the fracturing additives and/or the reservoir. All of the above drawbacks made water fracturing a cost-ineffective and environmentally risky process.[7, 8, 9, 10, 11]

Non-aqueous fracturing could be a potential solution

to circumvent the above issues.[12, 13] There are several technologies proposed already, such as high-energy gas fracturing (by a rapid burning of explosives or propellant),[13] foam fracturing (using a gas-liquid two-phase flow),[14] and even liquid nitrogen gasification fracturing.[15, 16] Among the proposed non-aqueous fracturing fluids, CO_2 is of particular interests.[2, 5, 17] This is because (1) CO_2 fracturing provided a potential solution to reservoirs located at arid areas by avoiding water usage[18]; (2) CO_2 fracturing may have lower breakdown pressure due to more effective activation of the pre-existing flaws[19, 20, 21, 22, 23]; (3) reservoir damage by aqueous fluids in water-sensitive formations, e.g., capillary blocking, can be avoided[24]; (4) oil/gas recovery can be enhanced by multiple mechanisms such as increasing miscibility of hydrocarbons, lowering viscosity of heavy oil, displacement of gas adsorbed on organic matters, and improving diffusivity[25, 26, 27]; and (5) part of the used CO_2 can be simultaneously stored in the formation after fracturing, enabling green and low-carbon production of unconventional resources.[28, 29, 30]

CO_2 fracturing can also be considered as an emerging technology in the portfolio of carbon capture, utilization, and storage (CCUS), similar to the enhanced oil recovery (EOR) and the enhanced coal-bed methane recovery (ECBM). As CCUS was predicted to be indispensable to achieve the carbon reduction target set by the Paris Accord,[31] related technologies are developing rapidly, making CO_2

fracturing cheaper and more feasible. For example, capturing CO_2 from industrial waste gas on a million-ton-per-year scale was recently demonstrated by the Boundary Dam CCS project and the Petro Nova CCS project.[32] This makes large-scale CO_2 fracturing a promising possibility for CO_2 utilization. On the other hand, as a downstream sector of carbon capture, CO_2 fracturing has promising potential to neutralize the cost of CO_2 capture.

To date, only very limited investigations on CO_2 fracturing were carried out. Researchers from Los Alamos National Laboratory performed systematic studies on CO_2 fracturing, including comprehensive analysis on fluid transport and influence on prolonged production. They predicted that CO_2 fracturing may be able to increase the cumulative production of shale gas by 80% in a 5-year-period. Consequently, the combinative benefits of CO_2 fracturing, i.e., enhancing production, CO_2 storage, less water dependent, etc., may considerably influence the industry of unconventional resource exploration.[5, 33] Ishida and co-workers found that comparing with water and liquid CO_2, supercritical CO_2 showed lower breakdown pressure but generated fractures that extended more three-dimensionally. They attributed these benefits to the low viscosity of supercritical CO_2,[34] which was supported by Deng and Yin's analysis based on linear elastic fracture mechanics.[23] A combined study of tri-axial experiments and computed tomography (CT)-scanning by Zhang and Lu et al.

also showed similar phenomena that, as compared with water fracturing, more than 50% decrease of initiation pressure and formation of more irregular cracks were achieved by CO_2 fracturing.[20]

Although the effectiveness of CO_2 fracturing over water is now recognized, lab experiments and field tests did not deliver positive results consistently.[5, 35] Fundamental understandings of CO_2 fracturing are still in their early infancy, and related publications are rare. In-depth knowledge from the perspective of how the unique properties of CO_2 can affect fracturing performance is still lacking. More importantly, the intrinsic mechanism and behavior of CO_2 fracturing across different length scales, as well as its comparison with water fracturing, remain the largest hindrance for practical application.

In order to fill the above blank, herein, we report a multiscale study on the comparison of water and CO_2 fracturing. To this end, a tri-axial fracturing rig coupled with *in situ* acoustic monitoring was specially designed, which tracks the dynamic fracturing process with unparallel time and space resolution. As such, the obtained data allowed us to perform simplified moment tensor analysis (sMTA) to quantitatively determine the fracturing mechanism. Furthermore, formation of fracture networks by CO_2 and water was investigated and simulated to study the difference in stimulated reservoir volume. It was found that CO_2 fracturing is highly effective in lowering breakthrough pressure while enhancing the

complexity of the fracture network. Such excellent behavior can be attributed to high leak-off that is closely related to the low viscosity and high mobility of CO_2. The laboratory investigation was complemented by data from field tests at Jilin oil field, where the tight oil production was not altered by water fracturing but could be enhanced significantly upon CO_2 fracturing.

Results and Discussion

Micro-scale: Breakthrough Pressure during CO_2 and Water Fracturing

Our first attempt is to investigate the difference in using CO_2 and water as fracturing fluids at the microscopic level. To this end, shale outcrops from the Longmaxi formation (Chongqing, SW China) were collected and processed into cylindrical samples. During the procedure, a surface layer of at least 20 cm was removed first to minimize the effect of weathering. Measurements were conducted to verify the mechanical properties of the collected outcrops, and core samples from the same formation are similar (Table S1). After fitting a simulating well to the samples, they were submitted to fracturing experiments in a tri-axial chamber at reservoir conditions. During the process, the initiation and propagation of fractures were monitored by *in situ* detection of acoustic emission (AE) signals. At the same time, injection pressure (IP) and flow rate (FR)

of the used fracturing fluid were recorded. Detailed experimental methodologies were described in Experimental Procedures and Supplemental Information 1 (Figures S1–S4).

First, a water fracturing experiment was performed under a confining pressure of 20 MPa and an axial load of 2 MPa. A programmed IP ramping of 500 kPa/min was used during the entire process. Under these conditions, however, the sample stayed intact even after applying an IP of 37.0 MPa (Figure 1A). Correspondingly, the AE results showed densely concentrated events at the close vicinity of the borehole (Figure 1B). CO_2 fracturing under the same condition was then carried out. As showed in Figure 1C, a high FR was observed at the initial injection stage because of the higher compressibility of CO_2. At ca. 2,600 s, instant decrease of IP accompanied by an increase of CO_2 FR was observable probably because of the propagation of fractures (blue circle). Such a high FR indicated that a larger volume of fluid was needed for CO_2 fracturing than that of water. Breakthrough was observed at ca. 2,800 s with an IP value of 28.0 MPa, 25.1% lower than the maximum IP observed in Figure 1A for water fracturing; note that breakthrough was not achieved in the latter case. More interestingly, we noted from the AE detection that cracks generated by CO_2 were more widely distributed even at a lower IP (Figure 1D), indicating a larger volume of the shale matrix can be pressurized by CO_2. As a control experiment, water

fracturing was carried out again by slightly increase the axial load to 5 MPa for proper sealing of the well (Figure 1E). It was found that upon injection of water (1.2 mL/min), IP built up almost linearly after an initial stage, and then suddenly decreased from 36.8 to 31.0 MPa (820 s), indicating accelerated formation of fractures. During this experiment, concentrated propagation of fractures was observed from the AE detection (Figure 1F), which eventually led to breakthrough of the sample at 38.6 MPa. This is to say that the breakthrough pressure for water fracturing is ca. 40% higher than that of CO_2 fracturing at similar conditions (Figure 1C). In addition, we found that by decreasing the pressure ramping rate to 250 kPa/min, the breakthrough pressure of CO_2 fracturing could be further lowered to 21.7 MPa, while the stimulated volume was not sacrificed (Figures 1G and 1H).

Figure thumbnail gr1

Figure 1 Water and CO_2 Fracturing of Cylindrical Shale Samples

∨ Show full caption

(A and B) IP, FR, and AE accumulation (A) and fracture location (B) during water fracturing (confining pressure, 20 MPa; axial load, 2 MPa; pressure ramping, 500 kPa/min).

(C and D) IP, FR, and AE accumulation (C) and fracture location (D) during CO_2 fracturing (confining pressure, 20 MPa; axial load, 2 MPa; pressure ramping, 500 kPa/min).

(E and F) IP, FR, and AE accumulation (E) and fracture location (F) during water fracturing (confining pressure, 20 MPa; axial load, 5 MPa; flow rate, 1.2 mL/min).

(G and H) IP, FR, and AE accumulation (G) and fracture location (H) during CO_2 fracturing (confining pressure, 20 MPa; axial load, 2 MPa; pressure ramping, 250 kPa/min).

View Large Image | Figure Viewer | Download Hi-res image | Download (PPT)

Fracturing mechanism was further studied by submitting the AE results to sMTA as the method determines the nature of fractures quantitatively rather than the qualitative visual observation (Supplemental Information 2; Figures S5 and S6).[36, 37] The results showed in Figure 2A indicated that, for water fracturing, only those fractures located at the borehole showed a diversified propagation direction. However, multi-directional development of fractures was observable at different locations of the CO_2 fractured sample (Figure 2B), indicating the potential to generate more complex fracture networks (*vide infra*). Very interestingly, we found that for CO_2 fracturing, over 85% of the analyzed fractures belong to shear type, while at least 30% of the fractures are contributed by tensile and mixed type for water fracturing (Figures 2C and 2D; Supplemental Information 3; Figures S7–S9). These results are in good agreement with those from Ishida et al., who reported that more shear fractures were generated

by using fluids with lower viscosity.[38] According to Šilený et al. and Cornet et al., pressure delivered by geofluids in natural porosity of a formation can substantially influence the fracturing behavior. With poor mobility, simple tensile fractures are more likely to form perpendicular to the minimum principal stress direction. In contrast, if the pores can be properly pressurized, a slip of the pre-existing natural fractures can be induced and thus trigger shear cracks.[39], [40]

Figure thumbnail gr2

Figure 2 **Fracturing Mechanism Analysis**

∨ Show full caption

(A and B) Position resolved sMTA during (A) water and (B) CO_2 fracturing; filtered AE events for sMTA were indicated by circular plates where the (1) position of the events was indicated by the center of the circular plates; (2) color of the plates suggested different modes of fracturing (red-shear crack, blue-tensile crack, and green- mixed- mode); (3) arrows on the plates revealed the motion direction of cracks, and plane of the plates represented the crack surfaces (perpendicular to the crack normal vectors); and (4) diameters of the plates were proportional to the source amplitude of the corresponding AE events.

(C and D) Time resolved sMTA of water (C) and CO_2 (D) fracturing; color indicates fractures with different mechanisms; number in parentheses shows percentage of each mechanism.

View Large Image | Figure Viewer | Download Hi-res image | Download (PPT)

Mesoscale: Fracture Networks Generated by Water and CO_2 Fracturing

During the fracturing of the cylindrical samples, breakthrough achieved by CO_2 made it possible to quantitatively evaluate the roughness of the fractured surface with high resolution by using a Zygo NewView 8300 interferometer. Several scanning locations with an area of 3,000 × 3,000 µm along the fracture path (determined by *in situ* AE detection) were selected to minimize any subjective factors. Among the analyzed areas, height differences as large as ca. 260 µm were obtained (Supplemental Information 4; Figures S10 and S11; Table S2). It should be noted that the surface complexity obtained in our study is considerably higher than that reported by Li and Feng et al.,[24] probably because of different experimental conditions and intrinsic properties of the used samples.

Nevertheless, results showed in Figure 1 are less favorable in reflecting the propagation of fractures because of the small size of the used samples. In this regard, larger samples (300 × 300 × 300 mm) were thus collected and fractured in a tri-axial system (Supplemental Information 5; Figures S12 and S13; Table S3). Similar to the aforementioned results in Figure 1, CO_2 fracturing showed lower breakthrough pressures than that of water. The post-fractured samples were characterized by 3D scanning, and the reconstructed breakthrough

surfaces are shown in Figure 3 (see Videos S1 and S2 for network demonstrations induced by CO_2 and water fracturing, respectively). Clearly, readily variation of the fracture direction could be observed in CO_2 fracturing, resulting in a more effective connection of natural fractures and thus formation of multiple and non-planar fracture networks (Figure 3A). On the other hand, fractures generated by water terminated easily when encountering bedding planes, any changing of propagation direction from one bedding plane was quenched quickly by merging into another bedding plane, leading to simple bi-wing fractures (Figure 3B).

Figure thumbnail gr3

Figure 3 **Reconstructed Fracturing Surface**

∨ Show full caption

(A) CO_2 fracturing.

(B) Water fracturing.

(C) Calculation of SA_{FiB}.

View Large Image | Figure Viewer | Download Hi-res image | Download (PPT)

[Download .mp4 (5.84 MB)](#)   [Help with .mp4 files](#)

Video S1. Network Demonstrations Induced by CO2 Fracturing

[Download .mp4 (9.12 MB)](#)   [Help with .mp4 files](#)

Video S2. Network Demonstrations Induced by Water Fracturing

Based on the digitalization of the fractured samples, the fracturing-induced breakthrough surface areas (SA_{FiB}) can be calculated ([Figure 3](#)C). Given perfect bi-wing splitting, an SA_{FiB} value of 1,800 cm^2 could be generated. Taking this value as a baseline, SA_{FiB}^{water} of water fracturing increased by only 7.4%, achieving 1,934 cm^2. Because the formation of more complex fracturing network by CO_2

fracturing, SA_{FiB}^{CO2} reached a promising value of 3,518 cm^2, corresponding to 95.4% and 81.9% increasing as compared to perfect bi-wing splitting and water fracturing, respectively. These results quantitatively evidenced that higher stimulated reservoir volume (SRV) can be achieved by CO_2, which would translate to more effective fracturing and enhanced oil/gas production due to larger drainage areas. In repeated experiments, the effectiveness of CO_2 fracturing was proved to be universal at different operational conditions and underground environments (Supplemental Information 5; Table S4; and Figures S14–S18). A general trend from these results showed that a larger *in situ* stress difference favors the formation of more complex networks.

Macro-scale: Enhancing Production of Tight Oil by CO_2 Fracturing

In the above laboratory experiments, outcrops were used because the processing of core shale samples with the appropriate size and avoiding its rapid weathering is extremely difficult. Although special cautions were taken during sample collection, and the geomechanical parameters of the outcrops were comparable to core samples from the same formation (Table S1 in Supplemental Information 1), the gap between laboratory observations and practical operations cannot be ruled out. To address this issue, field tests of dry CO_2 fracturing were carried out in the tight oil reservoir at Jilin oil field, NE

China. The formation possesses low porosity (avg. 11.97%) and low permeance (0.63 mD) together with a low concentration of acid-sensitive minerals (e.g. chlorite), making it highly suitable for CO_2 fracturing. It should be mentioned that water fracturing in these reservoirs induced very limited SRV probably because of water sensitivity (Supplemental Information 6; Figure S19), and thus the enhancement on production from water fracturing is negligible.

For the CO_2 fracturing operation, a total of five wells were drilled and tested, and a typical operational curve and general process parameters are shown in Figure 4A and Table S5 (Supplemental Information 6). Each operation included five steps, namely leak testing, fracturing, proppant transporting, well closing, and production. It should be mentioned that pure CO_2 was employed during fracturing to achieve effective stimulation, while in the proppant transporting stage, CO_2 thickened with a custom-made tri-block co-polymer were used to enhance proppant carrying. Such a combination can also lower the cost and environmental footprint of the process. The used CO_2 during fracturing and proppant transporting stage accounts for ca. 45% and 55% of the total injected CO_2, respectively.

Figure thumbnail gr4

Figure 4 **Dry CO_2 Fracturing at Jilin Oil Field**

⌄ Show full caption

(A) Variation of operational parameters during the fracturing process of well E.

(B) Oil production before and after CO_2 fracturing of well A–E.

(C and D) Top (C) and side (D) views of micro-seismic monitoring during the fracturing process of well E (injection point: 0 [East]), 0 [North], and 1590 [Depth]). Red: injection of pad fluid; Green: injection of proppant; Blue: injection of displacement fluid.

View Large Image | Figure Viewer | Download Hi-res image | Download (PPT)

To our delight, oil production increased by ca. 4- to 20-fold after the entire CO_2 fracturing process (Figure 4B). Note that although the previous water fracturing was carried out in different wells, their influence may not be negligible. This is because during the subsequent operation with CO_2, the network complexity might be enhanced because of the presence of simple but far-reaching fractures generated by previous water fracturing.[41] Nevertheless, as water fracturing resulted in little enhancement of production, the results showed in Figure 4B still demonstrated the great promise of CO_2 fracturing or, more strictly, water + CO_2 fracturing. We also carried out micro-seismic monitoring during the fracturing process. It was found that the SRV induced by CO_2 fracturing is ca. 2.5 times larger than that of water (Figures 4C and 4D), which is in accordance with the laboratory

experiments. These real-world results revealed that as compared to water fracturing, CO_2 fracturing is an important and greener alternative, particularly for reservoirs with water-sensitive formations, located at arid areas, or other conditions that making water fracturing less applicable.

Mechanism: The Effectiveness of CO_2 Fracturing

The effectiveness of CO_2 fracturing over that of water was also reported by others, and such results were related to the viscosity and interfacial tension of the fluids (Supplemental Information 7; Figure S20).[5, 34, 38, 42, 43, 44] However, understandings on the in-depth mechanism were rarely reported, and direct and *in situ* evidence during the fracturing process is particularly lacking. During the preparation of this paper, fracture propagation in CO_2 and water fracturing was comprehensively simulated and reported by Li and Zhang.[41] In their work, complexity of fracture networks generated by supercritical CO_2 is significantly higher than that of water. Correspondingly, the artificial fracture area induced by supercritical CO_2 reached 1.573×10^4 m^2, roughly an order of magnitude higher than that induced by water (2.469×10^3 m^2) under the same pressure conditions. More interestingly, shear fracture accounted for more than 90% by CO_2 fracturing, while the contribution from shear and tensile fracturing is approximately the same for water

fracturing.

Our experimental results echo perfectly to these theoretical predictions. Based on our AE results showed in Figure 1, it is very obvious that CO_2 has a significantly higher mobility within the shale matrix probably because of higher leak-off. This may be related to the low viscosity and low interfacial tension of CO_2. Similar to those discussed by Li and Zhang from a simulation perspective,[41] we attribute the effectiveness of CO_2 fracturing (lower breakthrough pressure, complex fracture network, larger SRV, etc.) to its higher leak-off. First, breakthrough is dictated by the volume increasing rate of a fracture (v_{frac}) and the fluid fed into that fracture (v_{fluid}); namely, breakthrough occurs when $v_{frac} > v_{fluid}$. Since higher leak-off improves the delivery of IP into the shale matrix, an *in situ* stress regime can be readily altered, leading to higher v_{frac}. At the same time, higher leak-off also slows the accumulation of fluid in a local fracture and thus lowers the v_{fluid}. Secondly, high leak-off allows filling of more beddings and/or natural cracks, and shear fractures could be more easily generated at these locations because of their lower cohesion strength. Accumulation of these shear events possibly lowered the pressure barrier for the formation of tensile and mixed fractures. This behavior could be verified by the accumulation of AE events during the experiments. As can be seen in water fracturing (Figures 1A and 1E), the generation of AE events accelerated only after substantially high IP (ca. 15 MPa). In contrast, a considerable amount

of AE events already generated at IP below 10 MPa during CO_2 fracturing (Figures 1C and 1G). Collectively, a combination of the above two factors eventually renders CO_2 fracturing with lower breakthrough pressures, more complex fracture networks, and larger SRV.

An issue that should be addressed is the interaction between natural and artificial fractures, which may become increasingly pivotal at the field scale. From Li and Zhang's simulation, discrepancies in viscosity and compressibility of CO_2 and water could lead to very different fracturing effectiveness with the presence of natural fractures.[41] In order to further verify such behavior, similar modeling was carried out under conditions closer to the Longmaxi formation. From Figure 5, it is clearly observable that CO_2 showed a greater tendency to penetrate natural cracks, leading to propagation of fractures within the rock matrix. On the other hand, cracks induced by water injection were favorably combined with natural fractures. These results are in good accordance with the experimentally observed formation of more complex networks and larger SRV by CO_2.

Figure thumbnail gr5

Figure 5 Fracturing Simulated by ABAQUS

⌄ Show full caption

Schematic fractures were magnified by 50 times for clarity; the red circles indicate injection points.

(A–C) Fracture network during water fracturing with injection time of 5.0 s (A), 11.6 s (B), and 20.0 s (C).

(D–F) Fracture network during CO_2 fracturing with injection time of 5.2 s (D), 11.5 s (E), and 20.0 s (F).

View Large Image | Figure Viewer | Download Hi-res image | Download (PPT)

Apart from the fluid itself, practical fracturing operation can also be influenced by a range of factors, which may affect the effectiveness of CO_2 and water fracturing. For example, it was reported that permeability of rock matrix can be altered substantially because of factors such as fracturing-induced roughness, adsorption and desorption of guests, and so on, and thus, the overall fracturing outcome in terms of production may vary.[45, 46] Therefore, further investigations are needed to identify the feasibility boundary of CO_2 fracturing technology, particularly the effects of types of reservoirs, geomechanical properties and conditions, CO_2 sensitivity of the formation, and so forth.

Conclusions

In summary, we report herein a multiscale investigation on dry CO_2 fracturing for the recovery of unconventional resources. It was found that as compared with the normally used water, CO_2 has higher leak-off within the natural porosity of the reservoir rock. This property enables better delivery

of IPs, resulting in an effective lowering of fracturing pressure. Moreover, thanks to the more accurate data collected by *in situ* AE monitoring, the fracturing mechanism can be quantitatively determined by sMTA. It was found that shear cracks were readily generated during CO_2 fracturing, which decreased the barrier for further formation of tensile and mixed fractures. Such microscopic behavior enabled the effective formation of more complex fracture networks on a mesoscale. We further report our observations in field tests that a 2.5 times higher stimulated reservoir volume was achieved by CO_2 fracturing as compared to water fracturing, resulting in a 4- to 20-fold increase in tight oil production. This disciplinary-crossing research provides comprehensive understandings on the mechanism and behavior of CO_2 fracturing and thus should shed meaningful lights on technologies of effective and greener recovery of unconventional resources, such as tight oil, shale gas/oil, etc.

Experimental Procedures

Fracturing of Cylindrical Shale and *In Situ* Acoustic Emission Monitoring

Cylindrical samples were obtained by collecting shale outcrops at Dayou Town; the formation belongs to the Lower Silurian Longmaxi marine shale

in southeastern Chongqing, SW China (Figure S1), Table S1 shows the general properties of the samples. The collected samples were first processed into cylindrical form with a diameter of 100 mm and a height of ca. 200 mm. During the sample collection and processing, a surface layer of at least 20 cm thickness was removed to avoid the influence of weathering. The representativeness of the outcrops was verified by comparing their mechanical properties with core samples from the same formation (Table S1). In the center of the sample, a hole (12 mm in diameter and ca. 80 mm in depth) was drilled. A stainless-steel (SS) tube of 6 mm diameter, with a grooved fitting for O-ring sealing, was inserted as a simulating well. The void between the well and the hole was then sealed by epoxy resin. An as-prepared sample was shown in Figure S2. During our experiments with the cylindrical samples, *in situ* AE monitoring was used as a direct and effective way to monitor the dynamic picture of the fracturing process. To this end, up to eight AE probes were assembled onto the surface of the samples, as showed in Figure S3. This enables the collection of the acoustic signals emitted by the initiation and propagation of fractures. Raw data were then subjected to an iterative localization algorithm to obtain dynamic, visualized, and position-resolved results of the fracturing process. The assembled sample was then placed onto the tri-axial chamber base, and an injection fitting was connected to the simulated well. The assembly showed in

Figure S3B was then sealed in a hydraulic chamber. Figure S4 shows the schematic diagram of the system. Into the hydraulic chamber, aviation hydraulic oil was pumped. After the temperature was controlled at 40°C by external heaters, the confining pressure was increased stepwise, and an additional load was applied in the axial direction. Fracturing of the samples was started by injection of either CO_2 (pre-heated to 40°C) or water into the well bore until drastic pressure drop was observed, which indicates either shale breakthrough or seal failure due to extremely high IPs (note: for CO_2 fracturing, a pre-injection stage with lower pressure ramping was used).

Large-Scale Tri-axial Fracturing

Large shale outcrop samples were collected from Lower Silurian Longmaxi Formation in Changning County, Sichuan Province (Figure S12). Table S3 shows the general properties of the samples. After removing the weathering layer, samples were processed into cubes of 300 × 300 × 300 mm in size. At the center of each cube, a hole with a diameter of 20 mm and a depth of 170 mm was drilled parallel to the bedding planes, and an SS tube (12 mm o.d.) was inserted as a simulating horizontal well and sealed similar to the cylindrical samples. A 1/8 inch tube was then welded and connected to an injection pump. Figure S13A shows the flowchart of the fracturing facility. A prepared sample was loaded into the tri-axial enclosure, and confining pressure was

gradually applied to levels of roughly one third of the reservoir conditions. After the loading was stabilized, water or CO_2 was injected with a programmed manner until sample breakthrough was achieved. The post-fractured samples were then characterized by 3D scanning via an EinScan S instrument. This method provides 3D coordinates of the breakthrough surface with a 0.1 mm resolution, and thus the digitalized samples can be reconstructed, and the fracturing-induced breakthrough surface areas can be calculated.

Field Testing

In the field testing, liquid CO_2 was first injected via a pre-cooled mixing unit and pipes (0°C ± 10°C). During this process, leak tests were performed by pressure pulse to higher than 30 MPa. After the fracturing process, a custom-made tri-block co-polymer bearing a perfluorinated carbon chain, sulfonate group, and styrene backbone was added (2 wt %, with <5 wt % acetone as a co-solvent) as a thickener. Because of the twinning and self-assembly of the polymer chain in CO_2, the viscosity of the fluid can be effectively increased to ca. 2 cP. This property allowed good transportation of proppants in the fluid, which is a very important concern for the practical application of CO_2 fracturing. After the operation, the injection well was closed for days before production was initiated.

ABAQUS Simulation

A numerical model in ABAQUS simulation was established by the fluid-solid coupling analysis module and cohesive element of ABAQUS. The natural fracture model was generated by Python with a cluster of conjugate natural cracks of 30° in dip angle. For the simulation with different fluids, pumping rates were kept identical while viscosity and leak-off coefficient were varied (see Supplemental Information 8 and Table S6 therein for detailed simulation parameters and source code).

Acknowledgments

Author Contributions

Conceptualization, W.W. and N.S.; Methodology, X.S., N.S., Y.G., and X.C.; Investigation, X.S., W.Y., W.C., G.S., Y.G., L.W., Jin Z., Jinhui Z., Xiaofeng L., Jun Z., and Z.X.; Resources, W.W., Z.T., and Xiao L.; Writing – Original Draft, N.S., X.S., Y.G., and Jin.Z.; Writing – Review & Editing, N.S., X.S., Y.G., and Jin.Z.; Funding Acquisition, W.W. and Xiao L.; Supervision, W.W. and Xiao L.

Declaration of Interests

The authors declare no competing interests.

Supplemental Information

📄

[Download .pdf (1.33 MB)](#)   [Help with pdf files](#)

Document S1. Figures S1–S20, Tables S1–S6, and Supplemental Experimental Procedures

References

1.   U.S. Energy Information Administration
     Annual Energy Outlook 2017.
     EIA, 2017

     View in Article ⌃   Google Scholar

2.   Wilkins R. • Menefee A.H. • Clarens A.F.
     Environmental life cycle analysis of water and CO$_2$-based fracturing fluids used in unconventional gas production.
     Environ. Sci. Technol. 2016; **50**: 13134-13141

View in
Article

Scopus (35) • PubMed • Crossref •

Google Scholar

3. Jeffrey L. • Garvin H. • Jordan M. • Elizabeth P. •
William B. • Ken C.
**Natural gas and the transformation of the U.S.
energy sector: electricity, technical report.**
NREL/TP, 2012

View in Article ⌃   Google Scholar

4. Burnham A. • Han J. • Clark C.E. • Wang M. •
Dunn J.B. • Palou-Rivera I.
**Life-cycle greenhouse gas emissions of shale
gas, natural gas, coal, and petroleum.**
Environ. Sci. Technol. 2012; **46**: 619-627

View in
Article

Scopus (467) • PubMed • Crossref •

Google Scholar

5. Middleton R.S. • Carey J.W. • Currier R.P. •
Hyman J.D. • Kang Q. • Karra S. •
Jiménez-Martínez J. • Porter M.L. •
Viswanathan H.S.
**Shale gas and non-aqueous fracturing fluids:
opportunities and challenges for supercritical
CO$_2$.**
Appl. Energy. 2015; **147**: 500-509

View in
Article

Scopus (607) • Crossref •

Google Scholar

6. Dehghanpour H. • Zubair H.A. • Chhabra A. •
    Ullah A.
    Liquid intake of organic shales.
    Energy Fuels. 2012; **26**: 5750-5758

    View in   Scopus (289) • Crossref •
    Article   Google Scholar

7. Montcoudiol N. • Isherwood C. • Gunning A. •
    Kelly T. • Younger P.L.
    **Shale gas impacts on groundwater
    resources: understanding the behavior of a
    shallow aquifer around a fracking site in
    Poland.**
    Energy Procedia. 2017; **125**: 106-115

    View in   Scopus (8) • Crossref •
    Article   Google Scholar

8. Rogala A. • Krzysiek J. • Bernaciak M. • Hupka J.
    **Non-aqueous fracturing technologies for
    shale gas recovery.**
    Physicochem. Probl. Miner. Process. 2013; **49**:
    313-321

    View in Article   Google Scholar

9. Zou C. • Dong D. • Wang Y. • Li X. • Huang J. •
    Wang S. • Guan Q. • Zhang C. • Wang H. •
    Liu H. • et al.
    Shale gas in China: characteristics,

challenges and prospects (II).
Petrol. Explor. Dev. 2016; **43**: 182-196

View in
Article

Scopus (269) • Crossref •

Google Scholar

10. Jasechko S. • Perrone D.
Hydraulic fracturing near domestic groundwater wells.
Proc. Natl. Acad. Sci. USA. 2017; **114**: 13138-13143

View in
Article

Scopus (43) • PubMed • Crossref •

Google Scholar

11. Llewellyn G.T. • Dorman F. • Westland J.L. • Yoxtheimer D. • Grieve P. • Sowers T. • Humston-Fulmer E. • Brantley S.L.
Evaluating a groundwater supply contamination incident attributed to Marcellus shale gas development.
Proc. Natl. Acad. Sci. USA. 2015; **112**: 6325-6330

View in
Article

Scopus (224) • PubMed • Crossref •

Google Scholar

12. Gupta, D.V.S. (2009). Unconventional fracturing fluids for tight gas reservoirs SPE Hydraulic Fracturing Technology Conference (SPE), p. 119424.

View in Article ⌃ Google Scholar

13. Li J. • Cao L. • Guo B. • Zhang X.

    Prediction of productivity of high energy gas-fractured oil wells.

    J. Petrol. Sci. Eng. 2018; **160**: 510-518

    View in Article ⌃   Scopus (20) • Crossref •

    Google Scholar

14. Faroughi S.A. • Pruvot A.J.-C.J. • McAndrew J.

    The rheological behavior of energized fluids and foams with application to hydraulic fracturing.

    J. Petrol. Sci. Eng. Review. 2018; **163**: 243-263

    View in Article ⌃   Scopus (67) • Crossref •

    Google Scholar

15. Li Z. • Xu H. • Zhang C.

    Liquid nitrogen gasification fracturing technology for shale gas development.

    J. Petrol. Sci. Eng. 2016; **138**: 253-256

    View in Article ⌃   Scopus (93) • Crossref •

    Google Scholar

16. Cha M. • Yin X. • Kneafsey T. • Johanson B. • Alqahtani N. • Miskimins J. • Patterson T. • Wu Y.-S.

    Cryogenic fracturing for reservoir stimulation

–laboratory studies.

J. Petrol. Sci. Eng. 2014; **124**: 436-450

View in Article   Scopus (207) • Crossref •

Google Scholar

17. Wang H. • Li G. • Shen Z.

A feasibility analysis on shale gas exploitation with supercritical carbon dioxide.

Energ. Source. A. 2012; **34**: 1426-1435

View in Article   Scopus (148) • Crossref •

Google Scholar

18. Yu W. • Lashgari H.R. • Wu K. • Sepehrnoori K.

CO_2 injection for enhanced oil recovery in Bakken tight oil reservoirs.

Fuel. 2015; **159**: 354-363

View in Article   Scopus (373) • Crossref •

Google Scholar

19. Zhou J. • Liu G. • Jiang Y. • Xian X. • Liu Q. • Zhang D. • Tan J.

Supercritical carbon dioxide fracturing in shale and the coupled effects on the permeability of fractured shale: an experimental study.

J. Nat. Gas Sci. Eng. 2016; **36**: 369-377

View in
Article

Scopus (124) • Crossref •

Google Scholar

20. Zhang X. • Lu Y. • Tang J. • Zhou Z. • Liao Y.
Experimental study on fracture initiation and propagation in shale using supercritical carbon dioxide fracturing.
Fuel. 2017; **190**: 370-378

View in
Article

Scopus (370) • Crossref •

Google Scholar

21. Liu F. • Ellett K. • Xiao Y. • Rupp J.A.
Assessing the feasibility of CO_2 storage in the New Albany Shale (Devonian–Mississippian) with potential enhanced gas recovery using reservoir simulation.
Int. J. Greenhouse Gas Control. 2013; **17**: 111-126

View in
Article

Scopus (211) • Crossref •

Google Scholar

22. Ishida T. • Aoyagi K. • Niwa T. • Chen Y. •
Murata S. • Chen Q. • Nakayama Y.
Acoustic emission monitoring of hydraulic fracturing laboratory experiment with supercritical and liquid CO_2.
Geophys. Res. Lett. 2012; **39**

View in Article

Scopus (284) • Crossref •

Google Scholar

23. Deng B. • Yin G. • Li M. • Zhang D. • Lu J. •
Liu Y. • Chen J.
Feature of fractures induced by hydrofracturing treatment using water and L-CO$_2$ as fracturing fluids in laboratory experiments.
Fuel. 2018; **226**: 35-46

View in Article

Scopus (68) • Crossref •

Google Scholar

24. Li X. • Feng Z. • Han G. • Elsworth D. •
Marone C. • Saffer D. • Cheon D.-S.
Breakdown pressure and fracture surface morphology of hydraulic fracturing in shale with H$_2$O, CO$_2$ and N$_2$.
Geomech. Geophys. Geo-energ. Geo-resour. 2016; **2**: 63-76

View in Article

Scopus (126) • Crossref •

Google Scholar

25. Liu J. • Yao Y. • Liu D. • Elsworth D.
Experimental evaluation of CO$_2$ enhanced recovery of adsorbed-gas from shale.
Int. J. Coal Geol. 2017; **179**: 211-218

View in Article

Scopus (112) • Crossref •
Google Scholar

26. Louk K. • Ripepi N. • Luxbacher K. • Gilliland E. •
Tang X. • Keles C. • Schlosser C. • Diminick E. •
Keim S. • Amante J. • et al.
**Monitoring CO_2 storage and enhanced gas
recovery in unconventional shale reservoirs:
results from the Morgan County, Tennessee
injection test.**
J. Nat. Gas Sci. Eng. 2017; **45**: 11-25

View in Article

Scopus (71) • Crossref •
Google Scholar

27. Lee T. • Bocquet L. • Coasne B.
**Activated desorption at heterogeneous
interfaces and long-time kinetics of
hydrocarbon recovery from nanoporous
media.**
Nat. Commun. 2016; **7**: 11890

View in Article

Scopus (114) • PubMed • Crossref •
Google Scholar

28. Molina O. • Vilarrasa V. • Zeidouni M.
**Geologic carbon storage for shale gas
recovery.**
Energy Procedia. 2017; **114**: 5748-5760

View in Article

Scopus (14) • **Crossref** •

Google Scholar

29. Schaef H.T. • Davidson C.L. • Owen A.T. •
Miller Q.R.S. • Loring J.S. • Thompson C.J. •
Bacon D.H. • Glezakou V.A. • McGrail B.P.
**CO_2 utilization and storage in shale
gas reservoirs: experimental results and
economic impacts.**
Energy Procedia. 2014; **63**: 7844-7851

View in Article

Scopus (63) • **Crossref** •

Google Scholar

30. Huo P. • Zhang D. • Yang Z. • Li W. • Zhang J. •
Jia S.
**CO_2 geological sequestration: displacement
behavior of shale gas methane by carbon
dioxide injection.**
Int. J. Greenhouse Gas Control. 2017; **66**: 48-59

View in Article

Scopus (86) • **Crossref** •

Google Scholar

31. International Energy Agency
Energy Technology perspectives 2017.
IEA, 2017

View in Article   **Crossref** • **Google Scholar**

32. Global Carbon Capture and Storage Institute

The Global Status of CCS.
GCCSI, 2017

View in Article ∧   Google Scholar

33. Middleton R.S. • Viswanathan H. • Currier R. •
Gupta R.
CO_2 as a fracturing fluid: potential for commercial-scale shale gas production and CO_2 sequestration.
Energy Procedia. 2014; **63**: 7780-7784

View in
Article   ∧   Scopus (128) • Crossref •
Google Scholar

34. Ishida T. • Chen Q. • Mizuta Y. • Roegiers J.
Influence of fluid viscosity on the hydraulic fracturing mechanism.
J. Energy Resour. Technol. 2004; **126**: 190-200

View in
Article   ∧   Scopus (156) • Crossref •
Google Scholar

35. Gupta D. • Bobier D.
The history and success of liquid CO_2 and CO_2/N_2 fracturing system.
SPE. 1998; : 40016

View in Article ∧   Google Scholar

36. Ohtsu M. • Ono K.

A generalized theory of acoustic emission and Green's functions in a half space.
J. Acoust. Emiss. 1984; **3**: 27-40

View in Article ∧   Google Scholar

37. Ohtsu M.
Simplified moment tensor analysis and unified decomposition of acoustic emission source: application to in situ hydrofracturing test.
J. Geophys. Res. 1991; **96**: 6211-6221

View in Article ∧   Scopus (270) • Crossref •
Google Scholar

38. Ishida T. • Chen Y. • Bennour Z. • Yamashita H.
Inui S. • Nagaya Y. • Naoi M. • Chen Q. •
Nakayama Y. • Nagano Y.
Features of CO_2 fracturing deduced from acoustic emission and microscopy in laboratory experiments.
J. Geophys. Res. Solid Earth. 2016; **121**: 8080-8098

View in Article ∧   Scopus (111) • Crossref •
Google Scholar

39. Šílený J. • Hill D.P. • Eisner L. • Cornet F.H.
Non–double-couple mechanisms of microearthquakes induced by

hydraulic fracturing.

J. Geophys. Res. 2009; **114**: B08307

View in
Article

Scopus (160) • Crossref •

Google Scholar

40. Cornet F.H.

The relationship between seismic and aseismic motions induced by forced fluid injections.

Hydrogeol. J. 2012; **20**: 1463-1466

View in
Article

Scopus (25) • Crossref •

Google Scholar

41. Li S. • Zhang D.

How effective is carbon dioxide as an alternative fracturing fluid?.

SPE. 2019; **24**

View in Article

Google Scholar

42. Montgomery C.T. • Smith M.B.

Hydraulic fracturing: history of an enduring technology.

J. Petrol. Technol. 2010; **62**: 26-40

View in Article

Crossref • Google Scholar

43. McHugh S.

Crack extension caused by internal gas

pressure compared with extension caused by tensile stress.
Int. J. Fract. 1983; **21**: 163-176

View in Article

Scopus (86) • Crossref •

Google Scholar

44. Fisher M.K. • Wright C.A. • Davidson B.M. •
Goodwin A.K. • Buckler W.S. • Steinsberger N.P.
Integrating fracture mapping technologies to optimize stimulations in the barnett shale.
SPE. 2002; : 7441

View in Article

Google Scholar

45. Wang G. • Wang K. • Wang S. • Elsworth D. •
Jiang Y.
An improved permeability evolution model and its application in fractured sorbing media.
J. Nat. Gas Sci. Eng. 2018; **56**: 222-232

View in Article

Scopus (52) • Crossref •

Google Scholar

46. Fang Y. • Elsworth D. • Ishibashi T. • Zhang F.
Permeability evolution and frictional stability of fabricated fractures with specified roughness.
J. Geophys. Res. Solid Earth. 2018; **123**: 9355-9375

View in
Article

Scopus (47)   • Crossref   •

Google Scholar

Article info

Publication history

Identification

Copyright

User license

ScienceDirect

Access this article on ScienceDirect

Figures

Graphical Abst… **Figure 1** Water …

Figure 2 Fractu… **Figure 3** Recon…

Figure 4 Dry C… **Figure 5** Fractu…

Related Articles

CellPress

f instagram in X wechat weibo youtube

LIFE & MEDICAL SCIENCES JOURNALS

Cell

Cancer Cell

Cell Chemical Biology

Cell Genomics

Cell Host & Microbe

Cell Metabolism

Cell Reports

Cell Reports Medicine

Cell Stem Cell

Cell Systems

Current Biology

Developmental Cell

Immunity

Med

Molecular Cell

AUTHORS

Submit article

Multi-Journal Submission

STAR Methods

Sneak Peek – Preprints

REVIEWERS

Information for reviewers

NEWS & EVENTS

Newsroom

Cell Symposia

Consortia Hub

Webinars

LabLinks

ABOUT

About Cell Press

Open access

COVID Hub

Sustainability

Inclusion and diversity

CONTACT

Contact us

Help & Support

CAREERS

Cell Press Careers

Scientific job board

ACCESS

Subscribe

Claim

Read-It-Now

Recommend to Librarian

Publication Alerts

COLLECTIONS

Best of Cell Press

Cell Press Reviews

Cell Press Selections

Neuron

Structure

American Journal of Human Genetics (*partner*)

Biophysical Journal (*partner*)

Biophysical Reports (*partner*)

Human Genetics and Genomics Advances (*partner*)

Molecular Plant (*partner*)

Molecular Therapy (*partner*)

Molecular Therapy Methods & Clinical Development (*partner*)

Molecular Therapy Nucleic Acids (*partner*)

Molecular Therapy Oncolytics (*partner*)

Plant Communications (*partner*)

Stem Cell Reports (*partner*)

Trends in Biochemical Sciences

Trends in Cancer

Trends in Cell Biology

Trends in Ecology & Evolution

Trends in Endocrinology & Metabolism

Trends in Genetics

Trends in Immunology

MULTIMEDIA

Cell Press Podcast

Cell Press Videos

Coloring and Comics

Figure360

Cell Picture Show

Research Arc

Nucleus Collections

SnapShot Archive

INFORMATION

For Advertisers

For Recruiters

For Librarians

Privacy Policy

Terms and Conditions

Accessibility

Trends in Microbiology

Trends in Molecular Medicine

Trends in Neurosciences

Trends in Parasitology

Trends in Pharmacological Sciences

Trends in Plant Science

PHYSICAL SCIENCES & ENGINEERING JOURNALS

Cell Reports Physical Science

Chem

Chem Catalysis

Device

Joule

Matter

Trends in Chemistry

MULTIDISCIPLINARY JOURNALS

Cell Reports Methods

Cell Reports Sustainability

Heliyon

iScience

One Earth

Patterns

STAR Protocols

Nexus (*partner*)

The Innovation (*partner*)

Trends in Biotechnology

Trends in Cognitive Sciences

The content on this site is intended for healthcare professionals and researchers across all fields of science.

Privacy Policy   Terms & Conditions   Accessibility   Help & Support   Contact

RELX™